1995

Coordination of Adsorbed Boron: A FTIR Spectroscopic Study

Chunming Su
USDA-ARS

Donald L. Suarez
USDA-ARS, donald.suarez@ars.usda.gov

Environ. Sci. Technol. 1995, 29, 302–311

Coordination of Adsorbed Boron: A FTIR Spectroscopic Study

CHUNMING SU* AND
DONALD L. SUAREZ
USDA-ARS, U.S. Salinity Laboratory, 4500 Glenwood Drive, Riverside, California 92501

We studied B adsorption on amorphous aluminum and iron hydroxides, allophane, and kaolinite as a function of pH and initial B concentration. Boron adsorption lowered the point of zero charge of all four adsorbents, implying specific adsorption (inner-sphere complexation) of B. We provided novel information on the coordination of B adsorbed at mineral–water interfaces by attenuated total reflectance Fourier transform infrared (ATR-FTIR) spectroscopy. The ATR-FTIR spectra of interfacial B species were influenced by pH and mineral type. Strong trigonal B and weak tetrahedral B bands of the asymmetric stretching mode were observed on the difference spectra at pH ≈7 for amorphous iron hydroxide, whereas both strong trigonal and tetrahedral B bands were found at pH ≈10. A strong IR band of asymmetric stretching of tetrahedral B shifted to higher frequencies in am-$Fe(OH)_3$ paste at both pH's relative to that of boric acid solution at pH 11. Trigonal B asymmetric stretching bands shifted to higher frequencies on the difference spectra for am-$Al(OH)_3$ and allophane at both pH's compared to that of boric acid solution at pH 7. Polymerization of B on mineral surfaces is shown to be possible. The results provide spectroscopic evidence that both $B(OH)_3$ and $B(OH)_4^-$ are adsorbed via a ligand exchange mechanism.

Introduction

Despite a wealth of studies on the partitioning of ions at interfaces between solids and liquids, direct structural information for adsorbed species on solid surfaces is generally lacking. This understanding of the mechanism of adsorption at the molecular level is essential for developing quantitative descriptions and predictions of many interfacial processes. Adsorption at solid–liquid interfaces significantly alters the mobility and availability of ions in the environment and affects the removal of trace contaminants from wastewaters or groundwater (*1*).

One means of studying adsorption mechanisms is to observe the mobility of individual particles suspended in an aqueous solution under an electric field by microelectrophoresis (*2*). Specifically adsorbing anions form inner-sphere surface complexes. Inner-sphere surface complexes contain no water molecules between the adsorbate anion and the surface functional groups (*3*). The point of zero charge (PZC) of variable charge minerals is shifted to a more acidic value following specific adsorption of anions (*2*). The information obtained from microelectrophoresis is, however, indirect with respect to determination of an adsorption mechanism. One of the inherent weaknesses of this technique is that only an effective surface charge can be deduced from electrophoretic measurements. If B adsorption occurs in the inner structure of a mineral such as spherical allophane, the adsorption is screened by the effective charge on the outside of the sphere and no effective change in electrophoretic mobility would be observed. Direct evidence from spectroscopic studies is necessary to verify the adsorption mechanisms suggested by indirect experimental results and surface speciation models (*4, 5*).

The commonly used spectroscopic methods used to probe interfaces, such as X-ray photoelectron, infrared transmission, and electron diffraction, require sample desiccation and high vacuum techniques that may change irreversibly the surface species of interest. Information obtained under such conditions may not be valid for an aqueous system (*4*). In contrast, attenuated total reflectance Fourier transform infrared (ATR-FTIR) spectroscopy overcomes these problems, and it has been applied successfully to study the partitioning of species in situ at solid–liquid interfaces. For example, Tejedor and Anderson (*6*) studied the in situ ATR-FTIR spectrum of goethite in aqueous suspension as a function of pH, ionic strength, background electrolyte composition (phosphate), and solid concentration. Biber and Stumm (*7*) were able to determine the surface coordination of salicylic acid on aluminum and iron oxides by in situ ATR-FTIR spectroscopy. Hunter and Bertsch (*8*) successfully monitored tetraphenylboron degradation kinetics on clay mineral surfaces by ATR-FTIR spectroscopy. Johnston and Sposito (*4*) concluded that ATR-FTIR is well suited to observe the interfacial chemistry of minerals in aqueous suspension. In the present study, the coordination of adsorbed boron species on the surfaces of amorphous aluminum and iron hydroxides, allophane, and kaolinite in aqueous solution have been determined using ATR-FTIR spectroscopy. The four minerals were chosen because they are abundant at the earth's surface and they play an important role in environmental mineral–water partitioning reactions. In addition, they are known

to adsorb significant amounts of B from aqueous solution (*9–11*).

Boron is of particular interest because it is both an essential element for plant growth and a toxic element in the environment, primarily to plants, if present in excess. The concentration range between plant deficiency and toxicity is the narrowest among all the micronutrients. It is necessary to understand the mechanism by which B is partitioned between mineral solids and soil solution since plants apparently respond only to the B activity in soil solution. Although ligand exchange has been proposed as a mechanism for B adsorption (*12*), it has not been verified satisfactorily by spectroscopic study. One reason for this is that direct analytical techniques for examining the chemistry of interfacial species have not been available until recently (*6*). In addition, the amount of B adsorbed is generally small compared to more strongly sorbed species such as phosphate. As a result, spectral subtraction is required to obtain surface complexed B signals in mineral–water pastes.

Study of the coordination of B on mineral surfaces is vital to understanding the adsorption mechanism. Some researchers have applied infrared transmission spectroscopy to study the coordination of B in synthetic B-containing minerals. For example, Stubican and Roy (*13*) showed that the increasing amount of B in tetrahedral sites in synthetic saponite obtained from fired glasses at 350 °C lowers the frequency and decreases the intensity of the infrared (IR) band in the frequency region 600–700 cm^{-1} due to the increase in the average (Si, B)–O distance. The same absorption band changes only slightly in frequency and intensity with the specimens obtained from gel (suspension), which indicates that the major quantity of B was not in tetrahedral sites in the gel-derived specimens. Jasmund and Linder (*14*) claimed to have obtained IR spectroscopy evidence that B in synthetic boron illites is located in tetrahedral positions since the strong band at 528 cm^{-1} was shifted up to 542 cm^{-1} upon B incorporation; however, no IR spectra were presented in their paper. The connection of B coordination in the mineral solids to this IR band is not straightforward, since the bending modes of both trigonally and tetrahedrally coordinated boron in borates give bands in the region of 700–400 cm^{-1} (*15*), and boric acid, which contains only trigonal boron, gives a strong band at 542 cm^{-1} for the BO_3 bending mode (*16*). Furthermore, since these B-containing minerals were synthesized at high temperature, the coordination of B within the structure of these minerals may be different from that which is present on the surface of minerals due to the adsorption process at ambient temperature. In contrast to these studies, some workers have postulated that B is adsorbed on mineral surfaces by forming four-coordinated complexes at ambient temperature. For example, Palmer et al. (*17*) using B isotope fractionation with pH (6.65–8.45) and temperature (5–40 °C) during the adsorption of B from seawater onto marine clays suggested that B is tetrahedrally coordinated on clay surfaces since $B(OH)_4^-$ is adsorbed more strongly than $B(OH)_3$. So far, no study has been reported on the use of ATR-FTIR spectroscopy to investigate in situ B complexes on the surfaces of adsorbents.

Materials and Methods

Preparation and Characterization of Materials. Amorphous aluminum hydroxide [am-$Al(OH)_3$] and iron hydroxide [am-$Fe(OH)_3$] were prepared by a modification of the method of Sims and Bingham (*18*). A total of 400 mL of 2.0 M NaOH was added at a rate of 50 mL min^{-1} to a stirred solution of 200 mL of 1.5 M $AlCl_3$. The pH at the end of the titration was 4.3. The precipitation product was washed four times with deionized water (DIW). At this point, dispersion started to occur as the electrical conductivity of the supernatant solution reached about 1 dS m^{-1}. The samples were subsequently air-dried. The mineral was ground to pass a 50-μm sieve. Amorphous iron hydroxide was prepared in a similar manner except that 450 mL of NaOH was added to 200 mL of 1.5 M $FeCl_3$ to reach an end point pH of 6.4 and then the DIW-washed precipitate was dried at 70 °C for 36 h and finally ground and sieved. An allophane with an Al/Si atomic ratio of 1.0 was synthesized by a modification of the method of Wilson et al. (*19*). A total of 200 mL of 0.1 M $AlCl_3$ was added at a rate of 5 mL min^{-1} to 200 mL of 0.1 M Na_2SiO_3 with constant stirring. The resulting mixture was adjusted to pH 8 with 1.0 M NaOH and then readjusted to this value after 14 h. When the pH was stable, solutions were further equilibrated for 5 d. The precipitate was centrifuged, washed first with DIW, then with 0.1 M NaCl three times, and then stored in 0.1 M NaCl. The material was verified to be X-ray amorphous. Kaolinite (KGa-2, poorly crystallized kaolinite) was obtained from the Clay Minerals Society's Source Clays Repository (University of Missouri, Columbia). DIW suspensions of kaolinite were adjusted to pH 9.5 with 1.0 M NaOH, and the < 2-μm fraction was separated by sedimentation. The clay-sized kaolinite was washed three times with 1.0 M NaCl, then with DIW three times, and finally with 0.1 M NaCl three times and then stored in 0.1 M NaCl. A quartz sample (Hot Springs, AR) obtained from Ward's Natural Science Establishment, Inc., (Rochester, NY) was ground and HCl-washed and DIW-rinsed. Then, the less than 2-μm fraction of the quartz was separated by sedimentation. The clay-sized quartz was repeatedly washed with 0.1 M NaCl and then stored in 0.1 M NaCl. A calcite sample from Baker Chemical Co. (reagent-grade $CaCO_3$) was obtained and used without any further treatment.

Specific surface areas of all the minerals except am-$Al(OH)_3$ were determined using a single-point BET N_2 adsorption isotherm on a Quantachrome Quantasorb Jr. surface area analyzer (Quantachrome Corp., Syosset, NY: Trade names are used only for the benefit of the reader and do not imply endorsement by the USDA). Samples of am-$Fe(OH)_3$ were degassed at 70 °C, and allophane, kaolinite, quartz, and calcite were degassed at 110 °C before determination of surface area. Surface area of am-$Al(OH)_3$ was determined by the ethylene glycol monoethyl ether (EGME) method (*20*) after desiccating the sample over P_2O_5 for 24 h. A preliminary experiment showed that the BET N_2 adsorption method was not suitable for am-$Al(OH)_3$, which was initially highly hydrated and apparently dehydrated and aggregated upon degassing under N_2 gas. The BET method gave an unrealistic low value (4–5 m^2 g^{-1}) for this material.

Adsorption Envelopes. Batch experiments were conducted for B adsorption at 25 and 5 °C to determine the amount of adsorbed B, as a function of solution pH, at fixed total B concentration in 0.1 M NaCl (adsorption envelopes). Samples of adsorbent (0.25 g for am-$Al(OH)_3$, am-$Fe(OH)_3$, and allophane and 0.5 g for kaolinite) were added to 30-mL polypropylene centrifuge tubes and equilibrated with 12.5 mL of 0.1 M NaCl containing $B(OH)_3$

either by shaking for 20 h on a reciprocating shaker at 25 °C or by occasional hand shaking in a water bath at 5 °C. The initial total B concentration was approximately 0.462 mmol of B L^{-1}. The suspension pH was adjusted to the desired levels with 1.0 M HCl or NaOH. The addition of HCl and NaOH caused less than a 8% change in the final volume. The supernatant solutions were separated by centrifugation at 7800*g* for 30 min at 25 or 5 °C, analyzed for pH, and then filtered through 0.1-μm Whatman filters. Boron concentration was determined using a Technicon autoanalyzer II (Technicon Industrial Systems, Tarrytown, NY) and the azomethine-H method described by Bingham (*21*). The amount of B adsorbed was calculated as the difference between the total B added and the B that remained in the aqueous solution. Calculation of adsorption was based on the 70 °C-dried mass for the hydroxides and on the 105 °C-dried mass for allophane and kaolinite. The volume of the equilibrium solution was gravimetrically determined. The adsorbents were examined by X-ray diffraction both before and after B adsorption.

Electrophoretic Mobility. The electrophoretic mobility (EM) was determined for all adsorbents except quartz and calcite with a Zeta-Meter 3.0 (Zeta Meter, Inc., Long Island, NY). Suspensions containing 0.2 g of solid L^{-1} in 0.1 M NaCl in the presence and absence of 23.1 mmol of B L^{-1} and with a final volume of 50 mL were shaken for 20 h at various pH levels. The suspension pH was adjusted with 0.1 M HCl or NaOH. At concentrations ≤25 mmol L^{-1}, essentially only mononuclear species $B(OH)_3$ and $B(OH)_4$ are present according to Cotton and Wilkinson (*22*). The suspension pH was determined before the EM measurement. In general, an average EM value was obtained after 30 particles were counted. The point of zero charge was determined by either obtaining zero EM or interpolating the data to zero EM.

FTIR Spectroscopy. Infrared spectra of solids, liquids, and pastes were recorded with a Bio-Rad FTS-7 FTIR spectrophotometer and a deuterated triglycine sulfate (DTGS) detector. For mineral solids, the traditional transmission method was used. IR spectra of the solids were recorded with samples diluted in KBr pellets. In each case, 200 mg of fine 105 °C-dried KBr powder was mixed with 0.1 mg of ground kaolinite or quartz; 0.5 mg of calcite; or 1 mg of am-$Al(OH)_3$, am-$Fe(OH)_3$, or allophane and pressed into 13-mm pellets. Infrared spectra were recorded with a CsI beam splitter from 4000 to 200 cm^{-1} at 4 cm^{-1} resolution over 1000 scans. The background spectrum of each KBr pellet was subtracted from the sample spectra.

Samples for ATR-FTIR spectroscopy consisted of either pure boric acid in 0.1 M NaCl or of mineral pastes obtained from centrifugation of equilibrated mineral–solution suspensions. Boric acid solutions of 4.62, 9.25, 23.1, and 92.5 mmol L^{-1} in 0.1 M NaCl electrolyte background prepared from CO_2-free water were adjusted to pH 7, 9, 10, and 11 with 1.0 M NaOH (CO_2-free). Mineral suspensions consisted of 0.25 g of either am-$Al(OH)_3$, am-$Fe(OH)_3$, allophane, 0.5 g of quartz, kaolinite, or calcite in 12.5 mL of 0.1 M NaCl adjusted to desired pH values near 7 and 10 and initial B concentrations. The inclusion of quartz and calcite in this experiment allowed us to compare band positions of B species in a nonadsorbent system with that of a strong adsorbent system and to determine the minimum concentration of B in a paste which can be detected with this instrument. Quartz and calcite were chosen because of the lack of IR bands in the region 1500–1300 and 1200–900 cm^{-1}, respectively. In addition, these minerals are stable, because quartz does not adsorb B and calcite shows only minimal adsorption of B. For the ATR-FTIR study using am-$Al(OH)_3$ and am-$Fe(OH)_3$, allophane, and kaolinite, the initial B concentrations used were 4.62, 9.25, and 23.1 mmol L^{-1}. Suspensions were equilibrated for 20 h at 25 °C, except for am-$Al(OH)_3$ at pH 10.2 ± 0.1, which was equilibrated at 5 °C. Preliminary experiments showed that for pH > 8.6 at 25 °C, am-$Al(OH)_3$ was largely transformed to pseudo-boehmite and bayerite, but remained amorphous at 5 °C for pH 3–11 after 20-h equilibration. Centrifugation was performed for 30 min at the corresponding temperature, and the solid to solution ratio was determined gravimetrically. The pH and B concentration were determined as above.

TABLE 1

Specific Surface Areas of Minerals Determined Using a Single Point BET N_2 Adsorption Isotherm for All Minerals Except am-$Al(OH)_3$, Which Was Determined by EGME Method[a]

material	surface area (m^2 g^{-1})
am-$Al(OH)_3$	128 ± 7
am-$Fe(OH)_3$	250 ± 3
allophane (Al/Si = 1)	201 ± 1
kaolinite (<2 μm)	20.2 ± 0.3
quartz (<2 μm)	6.6 ± 0.1
calcite (2–20 μm)	0.97 ± 0.02

[a] Values are for the average of two measurements and standard deviation.

Analyses of boric acid solutions with the reservoir module and mineral pastes with the pressure plate module of the horizontal ATR accessory were performed using horizontal ATR and an internal reflectance element (IRE) of ZnSe crystal. The crystal has dimensions of 85 × 10 × 10 mm^3 and is designed to have an average angle of light incidence of 45° and 16 reflections. In the reservoir module, the crystal was immersed in 4.5 mL of boric acid solutions. The reservoir was covered to prevent evaporative loss. In the pressure plate module, mineral pastes were spread on the ZnSe crystal and gently pressed and covered by the pressure plate. ATR-FTIR spectra were recorded from 4000 to 700 cm^{-1} at 4 cm^{-1} over 1000 scans.

All final ATR-FTIR spectra were the results of subtracting the spectra of the pH-adjusted 0.1 M NaCl solution or mineral paste without B (reference) from the spectra of the 0.1 M NaCl solution or paste with added B at the same pH (sample), both previously ratioed against the spectrum of the empty cell (background), respectively. The subtraction factor was set to equal 1.000. For the paste, the horizontal ATR accessory remained in place throughout the running of every spectra of the empty apparatus, reference, and sample so that its absorbance and average angle incidence were constant.

Results and Discussion

The surface areas of all the minerals except am-$Al(OH)_3$ listed in Table 1 were in reasonable agreement with literature values. The surface area decreased in the following order: am-$Fe(OH)_3$ > allophane > am-$Al(OH)_3$ > kaolinite > quartz > calcite.

Batch Equilibration Experiment. X-ray diffraction examination of minerals after B adsorption revealed that there was no crystalline phase detected at 25 °C for pH <

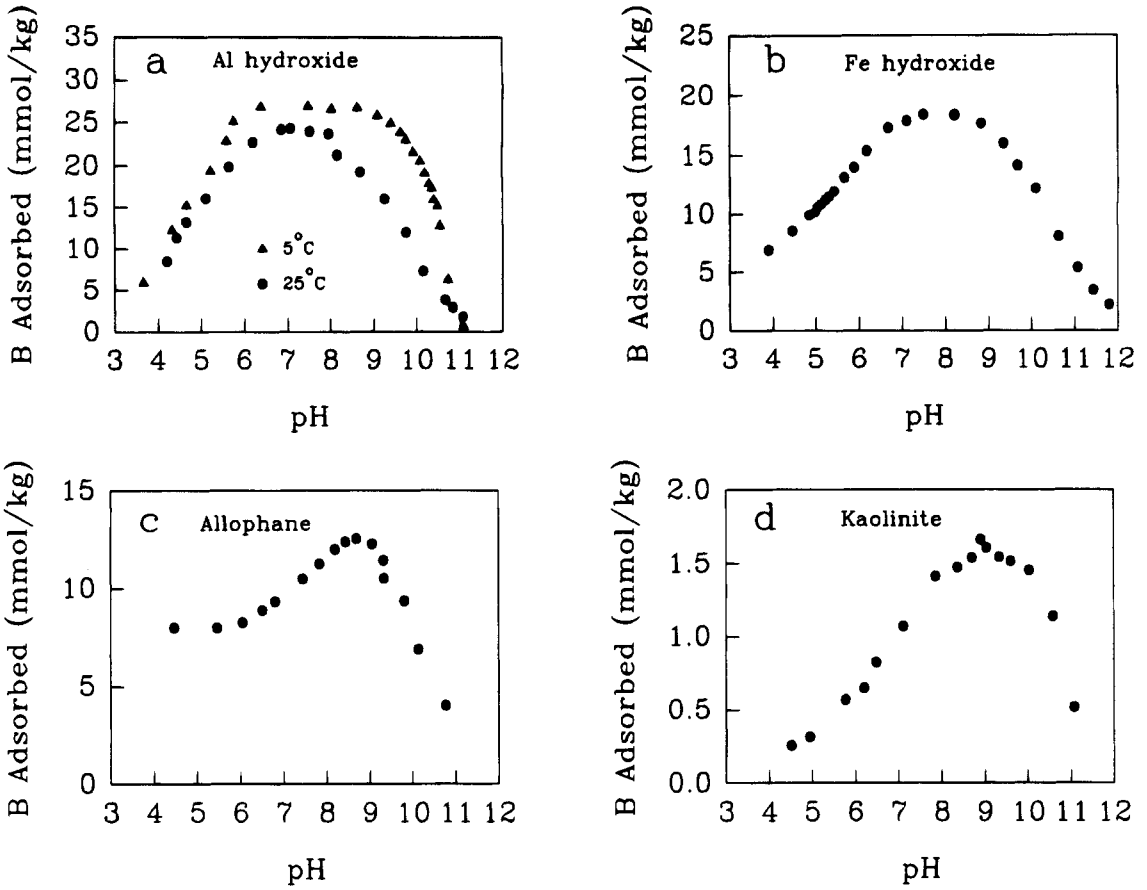

FIGURE 1. Boron adsorption in 0.1 M NaCl as a function of pH on (a) am-Al(OH)$_3$, (b) am-Fe(OH)$_3$, (c) allophane, and (d) kaolinite. The initial B concentration was approximately 0.462 mmol L^{-1}.

8.6 and at 5 °C for any pH in the am-Al(OH)$_3$ system. Am-Fe(OH)$_3$ and allophane remained X-ray amorphous after 20 h of reaction, and kaolinite was unchanged.

Boron adsorption envelopes from the batch system experiments are bell-shaped (Figure 1). Boron adsorption on am-Al(OH)$_3$ and am-Fe(OH)$_3$ increased from pH 3 to 6, showed a peak at pH 6.5–8.5, and decreased from 8.5 to 12. The adsorption maximum was located at pH 8–9 for allophane and at pH 8.5–9.5 for kaolinite. The maximum adsorption decreased on a mass basis in the order: am-Al(OH)$_3$ > am-Fe(OH)$_3$ > allophane > kaolinite. Goldberg and Glaubig (*23*) found a decreasing order in the maximum adsorption of B: am-Al(OH)$_3$ > am-Fe(OH)$_3$ > α-Al$_2$O$_3$ > goethite > hematite. Boron adsorption on am-Al(OH)$_3$ at pH 4–10.5 increased as temperature decreased from 25 to 5 °C. There was a larger range in the pH at which B adsorption exhibited maximum values at 5 °C than at 25 °C. Increased B adsorption with decreasing temperature for gibbsite, goethite, and kaolinite was reported by Goldberg et al. (*24*), who cited suggestions by Helferrich (*25*) that the highly specific adsorption of electrolyte ions is expected to be exothermic, implying an inner-sphere adsorption mechanism. Temperature affects the proportions and activities of the ions present in solution, the affinity of the ions for the surface, or the charge and therefore the potential of the surface (*26*). Although boric acid dissociation is slightly favored by an increase in temperature (pK_a = 9.24 at 25 °C vs pK_a = 9.44 at 5 °C for I = 0) (*27*), increasing temperature decreases the PZC for minerals (*26*). A decrease in PZC renders the surface more negative at a given pH and, therefore, decreases the adsorption of anions (*26*). Since the effect of change in surface charge is generally greater than the change in ion activities (*26*), the net result is that increasing temperature decreases adsorption of anions such as B(OH)$_4^-$. This, in turn, implies that B(OH)$_4^-$ could be the major species adsorbed on am-Al(OH)$_3$ surfaces at pH > PZC.

Microelectrophoresis. The presence of 23.1 mmol of B L^{-1} lowered the PZC value from 9.3 to 7.5 for am-Al(OH)$_3$, from 8.6 to 6.8 for am-Fe(OH)$_3$, from 7.8 to 6.0 for allophane, and from 3.0 to 2.3 for kaolinite, implying specific adsorption (inner-sphere complexation) of B in the solid–liquid interface (Figure 2). These results were consistent with previous experiments which showed a downward shift in PZC values following adsorption of B on pseudo-boehmite (*28*), Al(OH)$_3$ gel (*29*), magnetite (*30*), goethite (*31*), gibbsite, and kaolinite (*31*). It should be emphasized that no detailed adsorption mechanism can be derived solely and definitely from the information provided by microelectrophoresis due to the reasons presented in the Introduction.

Coordination of Adsorbed Boron. In order to identify the IR bands of trigonally and tetrahedrally coordinated boron in the solid–liquid interface, we analyzed ATR-FTIR spectra for boric acid solution as a function of pH and total B concentration (Figure 3). There is essentially no polynuclear B species present in solution at concentrations ≤25 mmol L^{-1} (*22*), and polynuclear species are less than 5% at pH 7 and less than 1% at pH 10 and 11, even at concentrations of 100 mmol L^{-1} (*32*). At pH 9, polynuclear species $B_3O_3(OH)_4^-$, $B_4O_5(OH)_4^{2-}$, and $B_5O_6(OH)_4^-$ account for only about 10%, 5%, and 1% of the total species at concentrations of 100 mmol L^{-1} (*32*). It is therefore assumed that the ATR-FTIR spectra for boric acid at pH 7, 9, 10, and 11 in the present study are dominated by mononuclear

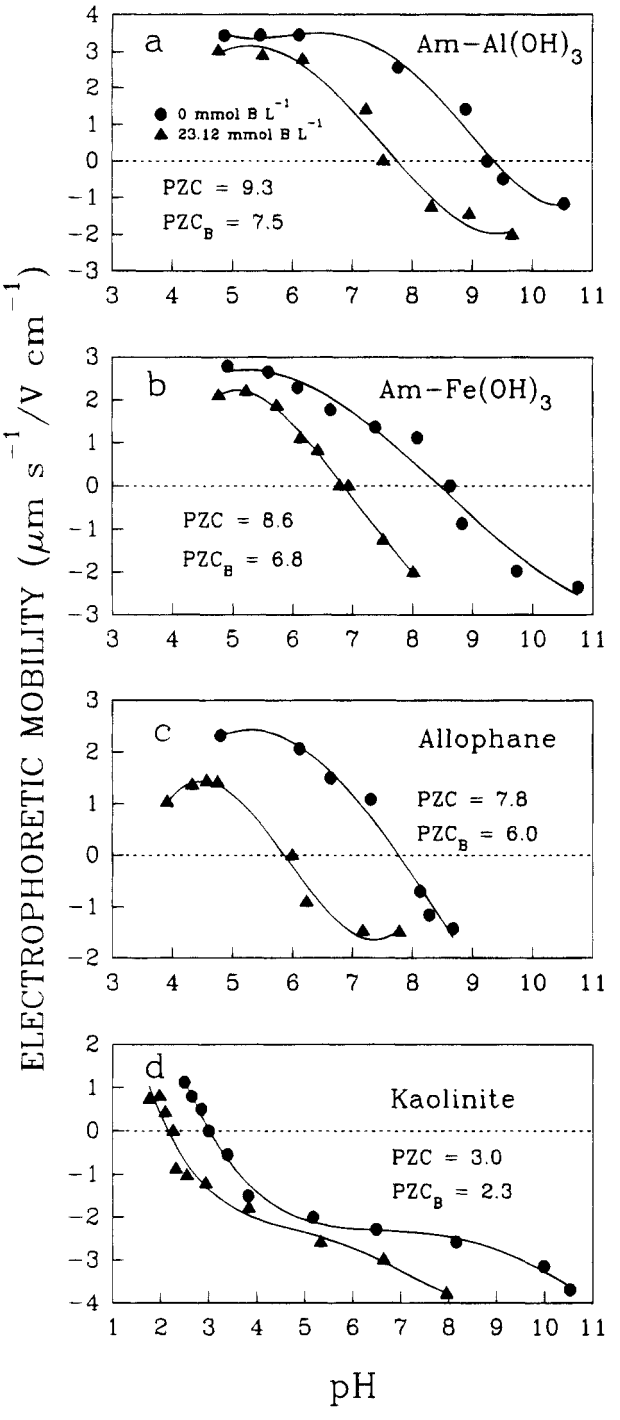

FIGURE 2. Effect of added boric acid on the electrophoretic mobility at 25 °C as a function of pH: (a) am-Al(OH)$_3$, (b) am-Fe(OH)$_3$, (c) allophane, and (d) kaolinite.

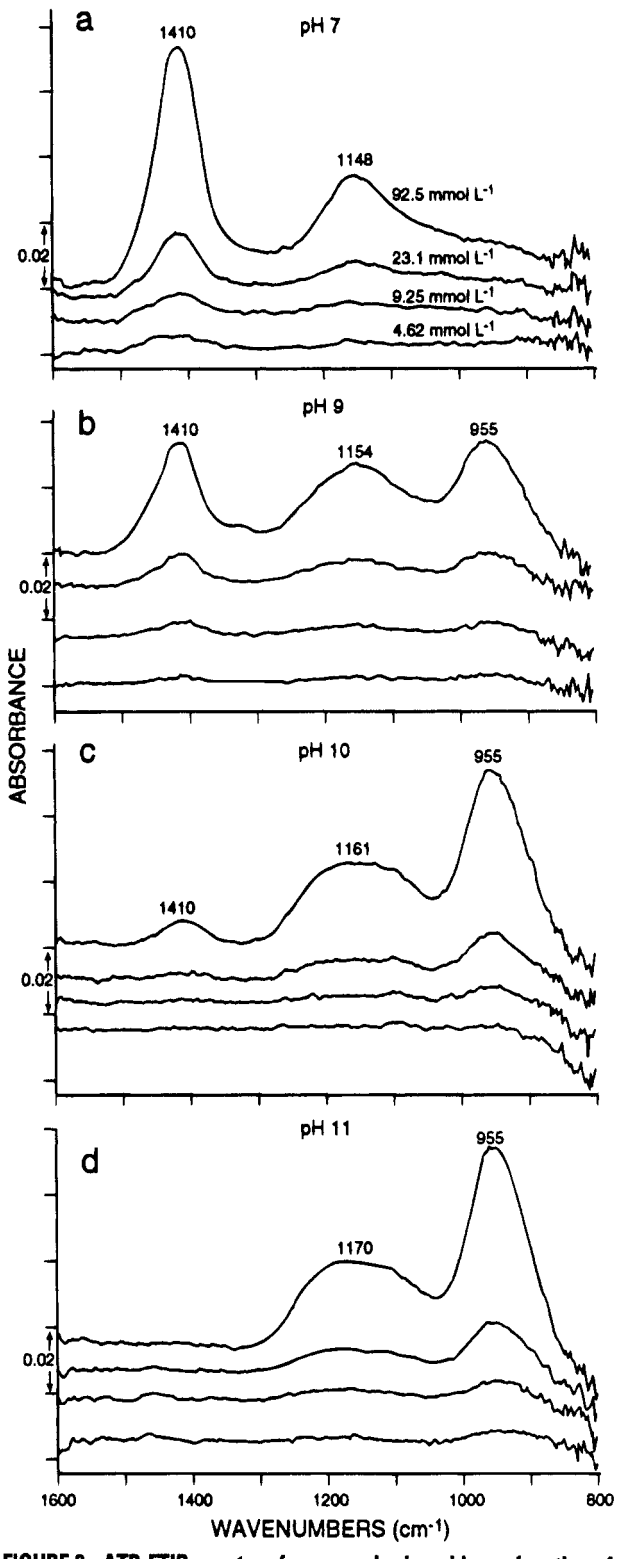

FIGURE 3. ATR-FTIR spectra of aqueous boric acid as a function of pH and total B concentration. Each spectrum is the difference between the sample (boric acid in 0.1 M NaCl at each pH) spectrum and the reference (0.1 M NaCl at the same pH) spectrum, both previously ratioed against the spectrum of the empty reservoir.

species. It has been established that the coordination polyhedron around a boron atom is either a triangle or a tetrahedron (*15*). All boron atoms in neutral boric acid molecules are trigonally coordinated. Dry boric acid is a planar molecule belonging to the symmetry point group C_{3h} (*33*). A lack of published IR data on boric acid solution prevents any comparison of the present work; the assignment of IR bands were based on published IR vibrational data for solid $B(OH)_3$ (*16*) and isotopic species of dry boric acid (*33*) of $B^{10}(OH)_3$, $B^{11}(OH)_3$, and $B^{11}(DH)_3$. The only broad bands at 1410 and 1148 cm^{-1} in Figure 3a are assigned to B-O asymmetric stretching of trigonal B and to B-OH in plane bending of trigonal B. These bands increase in intensity with increasing B concentration. At pH 9, which is near the pK_a for monomeric B species, roughly half of the total B is in the form of $B(OH)_3$ and half is in the form of the $B(OH)_4^-$ anion. The band at 955 cm^{-1} is assigned to asymmetric stretching of tetrahedral B, and the broad band at 1154 cm^{-1} in Figure 3b is a mixture of B-OH bending of both trigonal and tetrahedral B. As pH increases beyond 9, the $B(OH)_4^-$ anion becomes predominant (Figure 3c). At pH 11, 99.9% of the total B is in the tetrahedral form, which

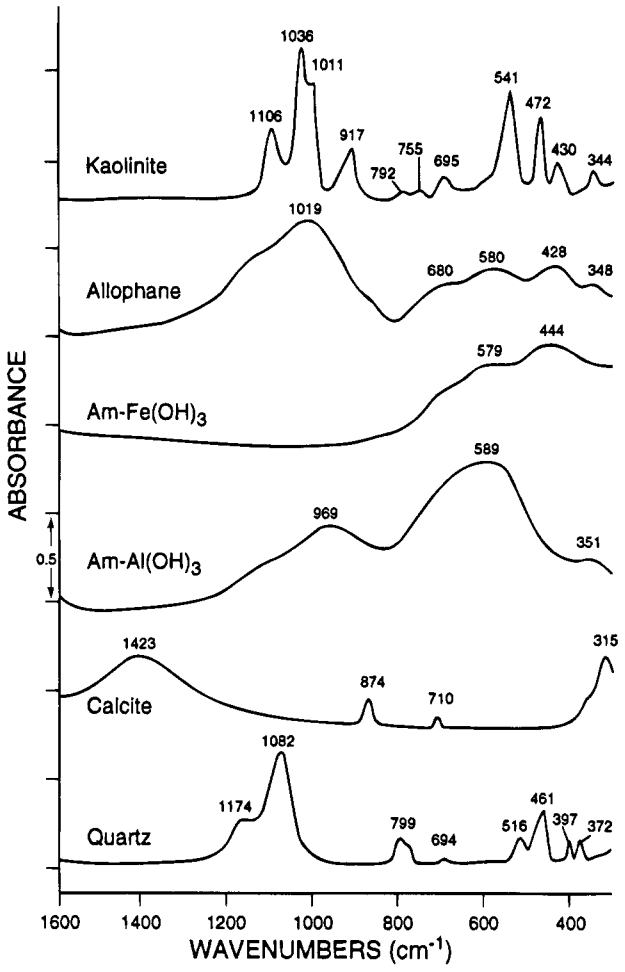

FIGURE 4. Transmission infrared spectra of dry mineral samples in KBr pellets (0.05% by weight for clay-sized quartz and kaolinite, 0.25% for calcite, and 0.5% for am-Al(OH)$_3$, am-Fe(OH)$_3$, and allophane). All minerals and KBr were dried at 105 °C for 24 h before pressing into pellets, except for am-Al(OH)$_3$ and am-Fe(OH)$_3$, which were dried at 70 °C to avoid phase change.

gives the same predominant band at 955 cm^{-1} (Figure 3d). The very broad band at 1170 cm^{-1} is assigned to B-OH bending of tetrahedral B. Based on the above data, we consider that the most useful diagnostic bands are at 1410 cm^{-1} for asymmetric stretching of trigonal boron and at 955 cm^{-1} for asymmetric stretching of tetrahedral boron. The published transmission IR spectra for solid-state borates (*15*) and borosilicates (*34*) are also in general agreement with the above assignments.

Figure 4 presents transmission IR spectra of the clay-sized quartz, calcite, and the four adsorbents, am-Al(OH), am-Fe(OH)$_3$, allophane, and kaolinite. The absence of IR bands in the 1600−1150 cm^{-1} region for all four adsorbents provides a suitable window for detecting trigonal boron on mineral surfaces if present at an adequate level. There is no strong band in the 1100−850 cm^{-1} region for am-Fe(OH)$_3$, making this material ideal for detecting tetrahedral boron on its surface. For the other three adsorbents, especially kaolinite, interference from the mineral makes the identification of tetrahedral boron very difficult. The absence of strong IR absorption bands in the region 1600−1250 cm^{-1} in clay-sized quartz and 1150−900 cm^{-1} in calcite is confirmed. The IR spectra of quartz and calcite are in good agreement with the reported spectra by Kodama (*35*). No interferences are expected for identifying asymmetric stretching of trigonal boron and asymmetric stretching of tetrahedral boron in quartz and calcite pastes, respectively. A preliminary experiment showed that quartz does not measurably adsorb boron at pH 7, where the neutral boric acid molecule is the dominant aqueous species. An additional experiment determined that calcite of surface area of 0.96 $m^2 g^{-1}$ adsorbs only a minimal amount of boron compared to amorphous aluminum and iron hydroxide(s) and allophane at pH 10−11, where the borate anion $[B(OH)_4^-]$ is the predominant aqueous species. These results are explained by the lack of active sites in quartz and by the low surface area of calcite. We found that the presence of quartz at pH 7 did not shift the trigonal asymmetric stretching band at 1410 cm^{-1} and calcite did not shift the tetrahedral B asymmetric stretching band at 955 cm^{-1}. The implication is that in the absence of specific adsorption of B there will not be any shift of aqueous B IR bands. Consequently, these two materials were used to determine the maximum concentration of boron in the aqueous phase of the mineral pastes, which would not cause interference in the IR spectra with the signals from the trigonally and tetrahedrally coordinated boron on the mineral surfaces. It is concluded that there is little interference until the boron concentration reaches 23.1 mmol L^{-1}.

Figure 5a presents the ATR-FTIR difference spectra of am-Al(OH)$_3$ paste at pH 6.8 ± 0.2 with adsorbed B for three initial B concentrations of 4.62, 9.25, and 23.1 mmol L^{-1}. The concentrations plotted next to the spectra in Figure 5a are the equilibrium B concentrations, which are far lower than the initial concentrations. The spectra indicate the presence of trigonal boron. Trigonal boron asymmetric stretching mode is indicated by a broad band centered at 1420 cm^{-1}, and trigonal boron B−OH bending mode is indicated by a band at 1280 cm^{-1}. Both bands were shifted to higher frequencies in the paste compared to the pure boric acid solution (1410 and 1148 cm^{-1}) at pH 7. This shift is likely due to the strengthening of O-B and B-OH bonds in the surface complex -Al-O-B(OH)$_2$ when the boric acid molecule is complexed with surface functional groups such as -Al-OH. Consistent with these being B adsorption bands (1500−1200 cm^{-1}), these bands increase in intensity with increasing boron adsorption. From 73 to 77% of the total added boron was adsorbed, producing final concentrations of boron in the aqueous phase far below 23.1 mmol L^{-1}. As a result, interference of IR bands of trigonally coordinated boron adsorbed on the surface with IR bands of trigonally coordinated boron in the aqueous phase was unlikely to have occurred in these systems. It is thus reasonable to state that the trigonal boron bands are largely due to adsorbed boron on the surface of am-Al(OH)$_3$.

Shown in Figure 5b is the ATR-FTIR difference spectra of an am-Al(OH)$_3$ paste with and without added B at pH 10.2 ± 0.1 and 5 °C. The B-O asymmetric stretching of trigonal B band at 1412 cm^{-1} was not significantly shifted compared to the 1410 cm^{-1} wavenumber for boric acid solution at pH 7, but the B-OH bending of trigonal B band had a narrower width and was shifted to a higher wavenumber of 1266 cm^{-1} from 1148 cm^{-1} due to the effect of B complexation on the mineral surface. Upon complexation, the B-OH bond is strengthened, and the B-OH bending frequency is increased. The higher absorbance of the band at 1266 cm^{-1} in Figure 5b than the absorbance of the band at 1280 cm^{-1} in Figure 5a is probably due to the lower solution to solid ratio in the paste at pH 10.2 (1.41 ± 0.14) than at pH 6.8 (2.00 ± 0.16). A lower ratio means

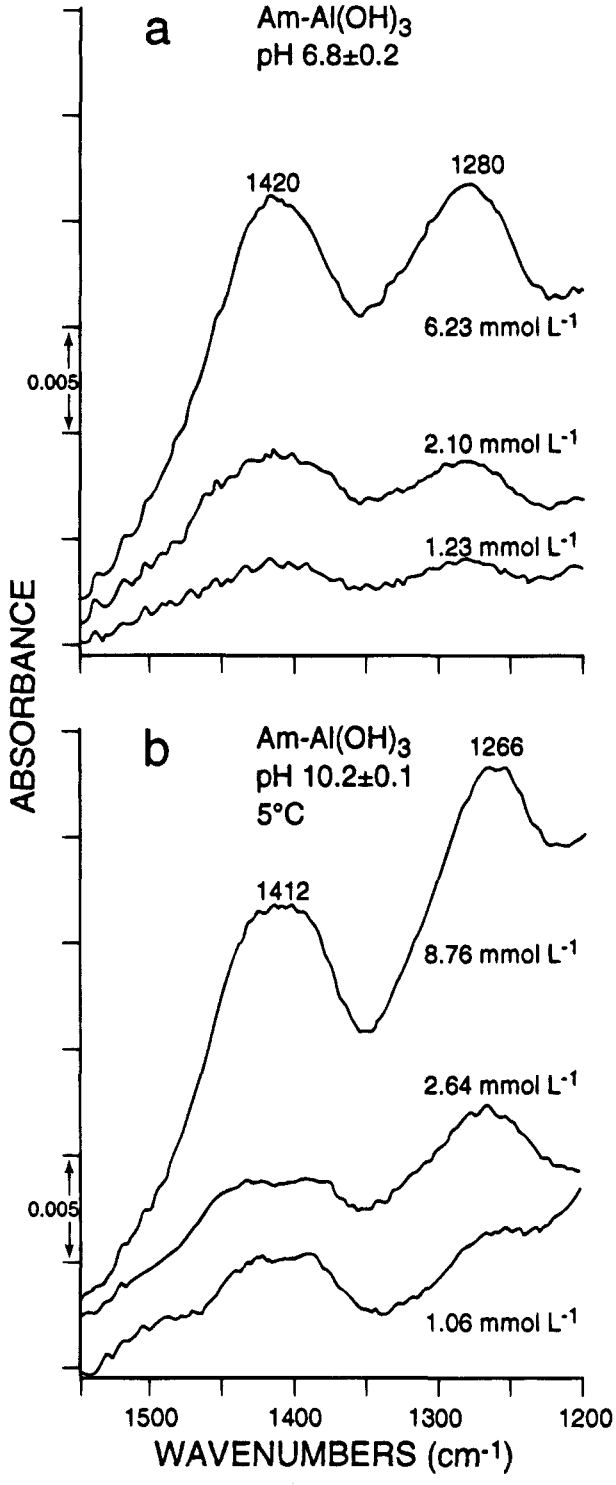

FIGURE 5. ATR-FTIR difference spectra of am-Al(OH)$_3$ paste: (a) at 25 °C in 0.1 M NaCl with a solution to solid mass ratio (R) of 2.00 ± 0.16 (n = 4) at pH 6.8 ± 0.2 (the spectrum of paste without B was subtracted from spectrum of paste with B). The equilibrium B concentration (C_e) of 1.23, 2.10, and 6.23 mmol L^{-1} correspond to B adsorption (Γ) of 209 mmol kg^{-1} and percentage of adsorbed B over total added B (θ) of 74%; Γ = 439 mmol kg^{-1} and θ = 77%; and Γ = 1040 mmol kg^{-1} and θ = 73%, respectively; (b) at 5 °C in 0.1 M NaCl with R = 1.41 ± 0.14 at pH 10.2 ± 0.1. Values of C_e of 1.06, 2.64, and 8.76 mmol L^{-1} correspond to Γ = 219 mmol kg^{-1} and θ = 77%; Γ = 407 mmol kg^{-1} and θ = 72%; and Γ = 880 mmol kg^{-1} and θ = 62%, respectively.

a higher amount of adsorbed B was exposed to the IR beam. Attempts to characterize tetrahedral B failed due to severe band interference in the range of 1000–900 cm^{-1} from the

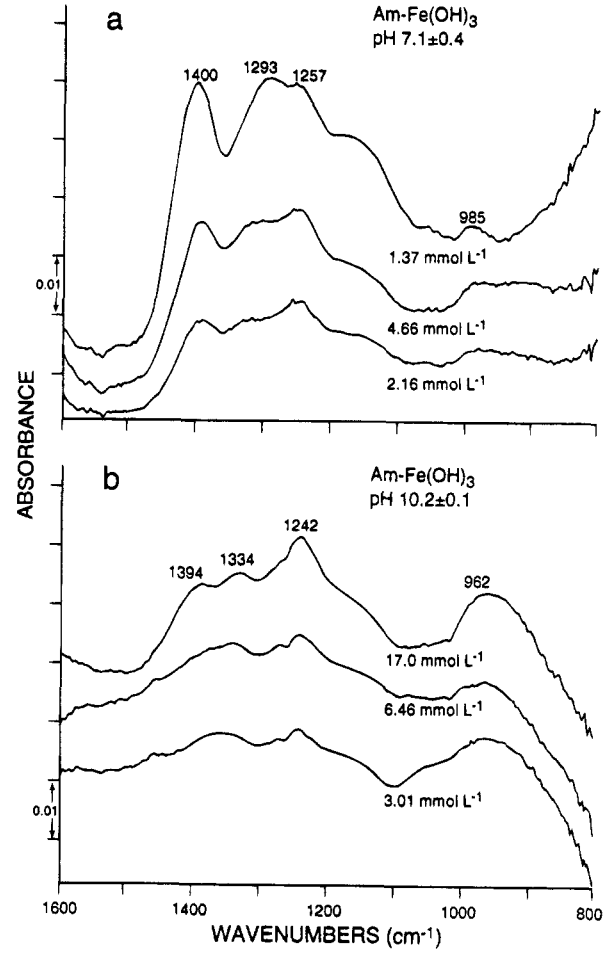

FIGURE 6. ATR-FTIR difference spectra of am-Fe(OH)$_3$ paste at 25 °C: (a) in 0.1 M NaCl with R = 0.93 ± 0.04 (n = 4) at pH 7.1 ± 0.4. The equilibrium B concentrations of 2.16, 4.66, and 13.7 mmol L^{-1} correspond to Γ = 128 mmol kg^{-1} and θ = 54%; Γ = 241 mmol kg^{-1} and θ = 51%; and Γ = 497 mmol kg^{-1} and θ = 42%, respectively; (b) in 0.1 M NaCl with R = 0.96 ± 0.04 at pH 10.2 ± 0.1. Values of C_e of 3.01, 6.46, and 17.0 mmol L^{-1} correspond to Γ = 85 mmol kg^{-1} and θ = 35%; Γ = 148 mmol kg^{-1} and θ = 30%; and Γ = 314 mmol kg^{-1} and θ = 26%, respectively.

Al-O bond, which has strong absorbance at 969 cm^{-1} (Figure 4). Although tetrahedral boron is the dominant species at pH 10.2 ± 0.1 in aqueous solution (Figure 3c), it need not be the dominant adsorbed species on am-Al(OH)$_3$ surfaces at that pH. The appearance of trigonal B on the surface of am-Al(OH)$_3$ at pH 10.2 suggests that the neutral B(OH)$_3$ species could be preferred due to its higher affinity for the negatively charged surface of am-Al(OH)$_3$ at high pH as compared to the B(OH)$_4^-$ ion, which would encounter charge repulsion. An alternative explanation is that polymerization of adsorbed B species occurs, resulting in both trigonally and tetrahedrally coordinated B.

Figure 6a shows a downward shift in the frequency region 1500–1400 cm^{-1} of asymmetric stretching of trigonal B on the surfaces of am-Fe(OH)$_3$ at pH 7.1 ± 0.4 compared to that on am-Al(OH)$_3$ at pH 6.8 ± 0.2 and to that of pure boric acid solution at pH 7. The band intensity at 1400 cm^{-1} increases with increasing B adsorption. In contrast, there is a upward shift in the frequency region 1350–1200 cm^{-1} for B-OH bending on the surface of am-Fe(OH)$_3$ as compared to am-Al(OH)$_3$ and pure boric acid solution at pH 7. Weak but well-defined and upward-shifted tetrahedral B asymmetric stretching band relative to 955 cm^{-1} of boric acid at pH 10 is also present at 985 cm^{-1} in the

spectrum for the highest B adsorption on am-$Fe(OH)_3$. At pH 10.2 ± 0.1, the am-$Fe(OH)_3$ paste gave different spectra (Figure 6b). It is evident that both trigonal and tetrahedral B were present on the mineral surfaces. The am-$Fe(OH)_3$ is the only material examined which has no bands that interfere with the tetrahedral B bands (see Figure 4). Bands at 1394, 1334, and 1242 cm^{-1} are attributed to trigonal B. The highest intensity band in the region 1450–1200 cm^{-1} was at 1242 cm^{-1}. The broad tetrahedral B band at 962 cm^{-1} was again shifted upward compared to 955 cm^{-1} in boric acid solution at pH 10.

Detection of IR bands of adsorbed B on aluminosilicates is more difficult than on am-$Fe(OH)_3$ due to the presence of Si-O bands. In the allophane paste at pH 7.2 ± 0.1 (Figure 7a), the trigonal B asymmetric stretching band at 1415 cm^{-1} increased only slightly in frequency compared to aqueous $B(OH)_3$ at pH 7. A shoulder at 1334 cm^{-1} may be assigned to the B-OH bending mode, which is also shifted upward in wavenumber. At pH 9.9 ± 0.3 (Figure 7b), the trigonal B-OH bending band at 1318 cm^{-1} was also shifted upward but to a lesser extent than in the pH 7.2 treatment shown in Figure 7a. It is difficult to identify tetrahedral B bands in allophane pastes due to severe band overlapping with the Si-O asymmetric stretching mode.

Due to the reason stated above, we were not successful in identifying tetrahedral B in the kaolinite paste; however, trigonal B signals at 1412 cm^{-1} at pH 7.1 ± 0.1 were obtained (not shown). Since the absorbance of the band is not much higher than the band for the quartz paste equilibrated with 23.1 mmol L^{-1} B, there is some uncertainty in assigning the band to adsorbed B species on the kaolinite surface. Resolution and reproducibility beyond the capability of our instrumentation would be needed to observe the small frequency shifts and the weak signal from the small amount of adsorbed B (low adsorption affinity of kaolinite).

Data in Table 2 summarizes the relative integrated absorption (IA) as described by Tejedor and Anderson (*36*) at different amounts of adsorbed B. Since the solid to solution ratios changed with pH for most samples due to differing water-holding capacity at different pH, the only valid comparison of IA values is for the same material at similar pH. Nevertheless, as expected, at each initial B concentration, IA for trigonal B (1500–1200 cm^{-1}) increased with increasing adsorbed B for amorphous hydroxides and allophane. The IA value for the tetrahedral B asymmetric stretching mode (1015–950 cm^{-1}) also increased for am-$Fe(OH)_3$.

Mechanism of Boron Adsorption on Mineral Surfaces. We propose possible chemical reactions for the formation of monomeric species of complexed B with mineral functional groups in the solid–liquid interface from adsorption envelopes, from electrophoretic mobility, and most importantly, from in situ ATR-FTIR spectra of adsorbed B species on mineral surfaces (Table 3). Reaction 1 depicts a condition at pH < PZC when the mineral surfaces are net positively charged and the neutral boric acid molecule is the predominant species in aqueous solution, and it is also presumed to be the preferred species to be adsorbed. This reaction is pH-dependent. An increase in pH would decrease the H^+ concentration and thus favor the forward reaction; however, an increase in pH would also decrease the concentration of SOH_2^+. As a result, a maximum adsorption of $B(OH)_3^0$ to form trigonally coordinated surface species occurs at a pH value, probably near the pK_a of boric acid for most adsorbents. As the pH

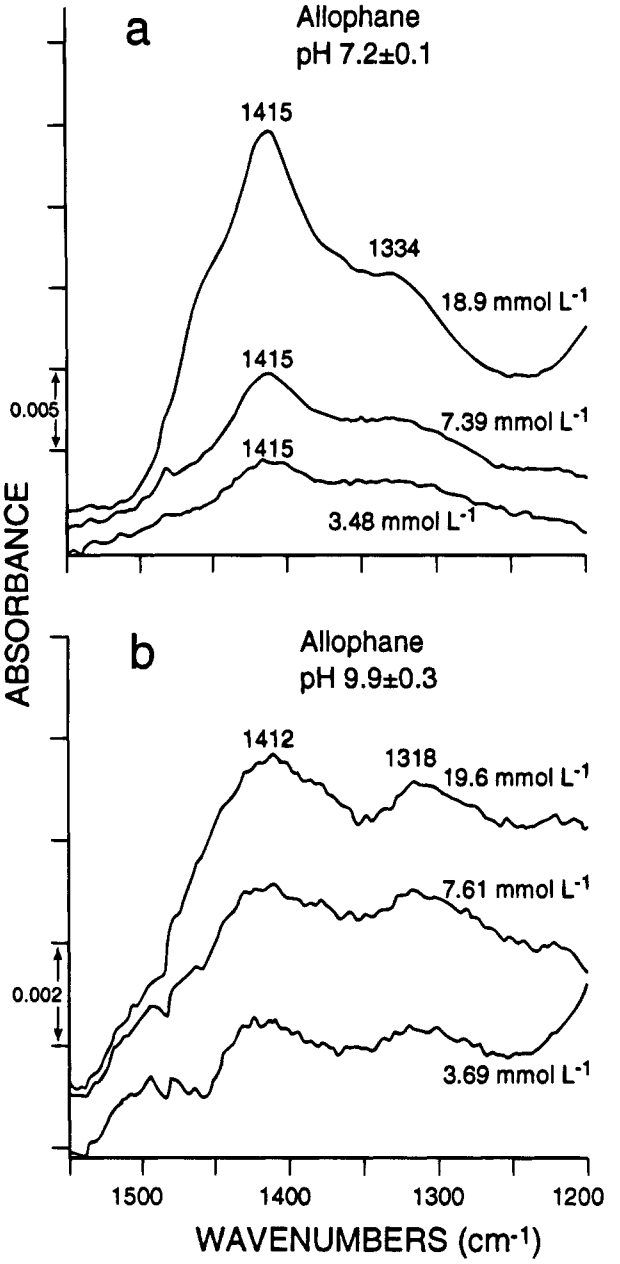

FIGURE 7. ATR-FTIR difference spectra of allophane paste at 25 °C: (a) in 0.1 M NaCl with $R = 8.18 \pm 0.06$ ($n = 4$) at pH 7.2 ± 0.1. The equilibrium B concentrations of 3.48, 7.39, and 18.9 mmol L^{-1} correspond to $\Gamma = 65$ mmol kg^{-1} and $\theta = 28\%$; $\Gamma = 109$ mmol kg^{-1} and $\theta = 23\%$; and $\Gamma = 247$ mmol kg^{-1} and $\theta = 21\%$, respectively; (b) in 0.1 M NaCl with $R = 8.30 \pm 0.06$ at pH 9.9 ± 0.3. Values of C_e of 3.69, 7.61, and 19.6 mmol L^{-1} correspond to $\Gamma = 49$ mmol kg^{-1} and $\theta = 35\%$; $\Gamma = 85$ mmol kg^{-1} and $\theta = 30\%$; and $\Gamma = 181$ mmol kg^{-1} and $\theta = 15\%$, respectively.

increases, the neutral surface functional group $SOH^0(s)$ becomes dominant, and reaction 2 could take place to produce the tetrahedrally coordinated B on the surface and to release H^+ to the solution. Monodentate complexes are indicated by reactions 1 and 3, and bidentate and binuclear complexes are indicated by reactions 2 and 4. At pH > pK_a of boric acid, the predominant species in aqueous solution is $B(OH)_4^-$, which also could be the preferred adsorbed species at high pH. Like $B(OH)_3$, adsorption of $B(OH)_4^-$ could also result in the formation of both trigonal and tetrahedral B species on mineral surfaces. At high pH, the mineral surfaces are net negatively charged, but the neutralspecies $SOH^0(s)$ should still be present. Reactions 5, 7, and 9 explain decreased adsorption at very high pH

TABLE 2

Relative Integrated Absorption (IA) as Function of Adsorbed B[a]

	initial B concentration (mmol L^{-1})		
	4.62	9.25	23.1
am-$Al(OH)_3$, pH 6.8 ± 0.2			
IA (1500–1200 cm^{-1})	0.205	0.649	1.683
B ads (mmol kg^{-1})	209	439	1040
am-$Al(OH)_3$, pH 10.2 ± 0.1			
IA (1500–1200 cm^{-1})	0.303	0.650	1.300
B ads (mmol kg^{-1})	219	407	880
Am-$Fe(OH)_3$, pH 7.1 ± 0.4			
IA (1500–1200 cm^{-1})	1.666	3.144	4.663
IA (1015–950 cm^{-1})	0.054	0.084	0.091
B ads (mmol kg^{-1})	128	241	497
am-$Fe(OH)_3$, pH 10.2 ± 0.1			
IA (1500–1200 cm^{-1})	0.726	1.073	1.740
IA (1050–900 cm^{-1})	0.394	0.366	0.567
B ads (mmol kg^{-1})	85	148	314
allophane, pH 7.2 ± 0.1			
IA (1500–1200 cm^{-1})	0.669	0.951	2.173
B ads (mmol kg^{-1})	65	109	247
allophane, pH 9.9 ± 0.3			
IA (1500–1200 cm^{-1})	0.234	0.628	0.855
B ads (mmol kg^{-1})	49	85	181

[a] The IA is the area under the IR bands and above the base lines as defined by Tejedor and Anderson (*36*).

TABLE 3

Possible Monomeric Surface Complexes of Boron with Mineral Functional Groups[a]

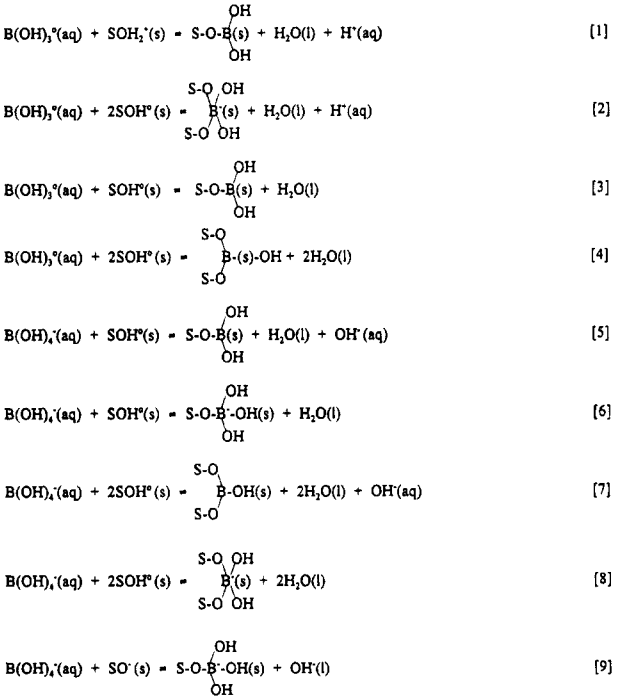

[1] $B(OH)_3°(aq) + SOH_2^+(s) = S\text{-}O\text{-}B(OH)_2(s) + H_2O(l) + H^+(aq)$

[2] $B(OH)_3°(aq) + 2SOH°(s) = (S\text{-}O)_2B\text{-}OH(s) + H_2O(l) + H^+(aq)$

[3] $B(OH)_3°(aq) + SOH°(s) = S\text{-}O\text{-}B(OH)_2(s) + H_2O(l)$

[4] $B(OH)_3°(aq) + 2SOH°(s) = (S\text{-}O)_2B\text{-}OH(s) + 2H_2O(l)$

[5] $B(OH)_4^-(aq) + SOH°(s) = S\text{-}O\text{-}B(OH)_2(s) + H_2O(l) + OH^-(aq)$

[6] $B(OH)_4^-(aq) + SOH°(s) = S\text{-}O\text{-}B(OH)_2\text{-}OH(s) + H_2O(l)$

[7] $B(OH)_4^-(aq) + 2SOH°(s) = (S\text{-}O)_2B\text{-}OH(s) + 2H_2O(l) + OH^-(aq)$

[8] $B(OH)_4^-(aq) + 2SOH°(s) = (S\text{-}O)_2B(OH)_2(s) + 2H_2O(l)$

[9] $B(OH)_4^-(aq) + SO^-(s) = S\text{-}O\text{-}B(OH)_2\text{-}OH(s) + OH^-(l)$

[a] Capital S represents a metal cation (Al or Fe) near the mineral surface. Lower case letters s, l, and aq represent solid, liquid, and aqueous phases, respectively.

due to competitive adsorption of $B(OH)_4^-$ and OH^- for surface sites. The only reactions which are consistent with both ATR-FTIR spectra and electrophoretic mobility data are 1, 2, 6, and 8. These reactions show the presence of both trigonal and tetrahedral B on the surface and indicate

TABLE 4

Percentages of Mineral Surfaces Occupied by Adsorbed Boron, Assuming Both $B(OH)_3$ and $B(OH)_4^-$ Have Area of 20 $Å^2$

		initial B concentration (mmol L^{-1})		
material	pH	4.62	9.25	23.1
am-$Al(OH)_3$	6.8 ± 0.2	19.8	41.6	98.1
	10.2 ± 0.1	20.9	38.5	83.2
am-$Fe(OH)_3$	7.1 ± 0.4	6.2	11.6	24.0
	10.2 ± 0.1	4.1	7.2	15.2
allophane	7.2 ± 0.1	3.9	6.5	14.8
	9.9 ± 0.3	3.0	5.1	10.9
kaolinite	7.0 ± 0.1	1.7	4.2	4.4
	10.2 ± 0.1	2.8	6.1	11.3

that B adsorption lowers the net surface charge on adsorbent particles. This study does not support the suggestion of Palmer et al. (*17*) that B forms only tetrahedrally coordinated complexes on mineral surfaces. Our results indicate that both trigonally and tetrahedrally coordinated complexes of B exist and that their relative proportion depends on pH and mineral type.

The adsorption of polynuclear species of B from aqueous solution is not likely the predominant process in this study since the initial B concentration was less than 25 mmol L^{-1} (*22*); however, the polymerization of adsorbed B on mineral surfaces cannot be completely disregarded. Data in Table 4 demonstrate that mineral surface coverage by adsorbed B increased with increasing initial B concentration at both pH levels; at each initial B concentration, the surface coverage increased in the order am-$Al(OH)_3$ > am-$Fe(OH)_3$ > allophane > kaolinite. The same order was shown above for the maximum adsorption of B expressed on an adsorbent mass basis. Most noteworthy is the magnitude of the surface coverage. Almost all of the surface of am-$Al(OH)_3$ and a quarter of the surface of am-$Fe(OH)_3$ were occupied by adsorbed B at near-neutral pH at an initial B concentration of 23.1 mmol L^{-1}. The high surface coverage by adsorbed B implies polylayer coverage or polymerization, since a single layer of monomeric boron would not expected to cover such a large fraction of the mineral surface, especially on the hydroxides. Because boric acid significantly forms a series of polyanions in solution at a total concentration greater than 25 mmol L^{-1} at pH 7.5–9 (*22*, *32*), it is speculated that the adsorption process may represent a surface-promoted polymerization on minerals. Based on the data in Table 4 and more importantly on the ATR-FTIR spectra of am-$Fe(OH)_3$, which showed the presence of both trigonally and tetrahedrally coordinated boron on mineral surfaces, we suggest that polynuclear B species on mineral surfaces may exist, especially on amorphous aluminum and iron hydroxides and allophane. This suggestion is supported by the ATR-FTIR spectra of adsorbed B, which showed that tetrahedral B was present even at pH < 7 and trigonal B at pH > 10. Possible polymeric boron complexes with mineral functional groups are presented in Table 5. Their formation does not violate the rules governing formation of hydrated borate polyanions proposed by Christ and Clark (*37*).

Conclusions

This study confirmed that B adsorption is dependent on pH, temperature, B concentration, and mineral type. Boron adsorption maximum occurred at pH 6.5–8.5 for amor-

TABLE 5

Possible Polymeric Boron Complexes with Mineral Functional Groups in Aqueous Mineral Paste

Dimer

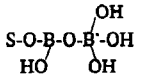

Trimer

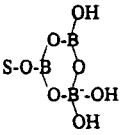

Tetramer

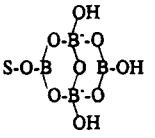

phous aluminum and iron hydroxides, 8–9 for allophane, and 8.5–9.5 for kaolinite. At maximum adsorption pH range, B adsorption decreased in the order: am-$Al(OH)_3$ > am-$Fe(OH)_3$ > allophane > kaolinite. The presence of 23.1 mmol B L^{-1} lowered the surface charge of all four minerals, implying inner-sphere complexation with mineral functional groups.

This paper reports for the first time on the coordination of adsorbed boron on mineral surfaces. Both $B(OH)_3^0$ and $B(OH)_4^-$ species are adsorbed via a ligand exchange mechanism. Polymerization of adsorbed B to give both trigonally and tetrahedrally coordinated boron on mineral surfaces is also likely to occur.

Literature Cited

(1) Stumm, W. *Chemistry of the Solid-Water Interface, Processes at the Mineral-Water and Particle-Water Interface in Natural Systems;* Wiley: New York, 1992; pp 87–155.
(2) Hunter, R. J. *Foundations of Colloid Science;* Oxford: New York, 1989; Vol. 2, pp 709–785.
(3) Sposito, G. *The Surface Chemistry of Soils;* Oxford: New York, 1984; p 13.
(4) Johnston, C. T.; Sposito, G. *Future Developments in Soil Science Research;* Soil Science Society of America: Madison, WI, 1987; pp 89–99.
(5) Davis, J. A.; Hayes, K. F. In *Geochemical Processes at Mineral Surfaces;* Davis, J. A., Hayes, K. F., Eds.; ACS Symposium Series 323; American Chemical Society: Washington, DC, 1986; pp 2–18.
(6) Tejedor, M. I.; Anderson, M. A. *Langmuir* **1986,** *2,* 203.
(7) Biber, M. V.; Stumm, W. *Environ. Sci. Technol.* **1994,** *28,* 763.
(8) Hunter, D. B.; Bertsch, P. M. *Environ. Sci. Technol.* **1994,** *28,* 686.
(9) McPhail, M.; Page, A. L.; Bingham, F. T. *Soil Sci. Soc. Am. Proc.* **1972, 36,** 510.
(10) Bingham, F. T.; Page, A. L.; Coleman, N. T.; Flach, K. *Soil. Sci. Soc. Am. Proc.* **1971,** *35,* 546.
(11) Singh, S. P. N.; Mattigod, S. V. *Clays Clay Miner.* **1992,** *40,* 192.
(12) Goldberg, S. In *Boron and Its Role in Crop Production* Gupta, U. C., Ed.; CRC Press: Boca Raton, FL, 1993; pp 3–44.
(13) Stubican, V.; Roy, R. *Am. Mineral.* **1962,** *47,* 1166.
(14) Jasmund, K.; Lindner, B. *Proc. Int. Clay Conf.* **1972,** *1973,* 399.
(15) Ross, S. D. In *The Infrared Spectra of Minerals;* Farmer, V. C., Ed.; Mineralogical Society: London, 1974; Chapter 11, pp 205–226.
(16) Durig, J. R.; Green, W. H.; Marston, A. L. *J. Mol. Struct.* **1968,** *2,* 19.
(17) Palmer, M. R.; Spivack, A. J.; Edmond, J. M. *Geochim. Cosmochim. Acta* **1987,** *51,* 2319.
(18) Sims, J. R.; Bingham, F. T. *Soil Sci. Soc. Am. Proc.* **1968,** *32,* 364.
(19) Wilson, W. A.; McCarthy, S. A.; Fredericks, P. M. *Clay Miner.* **1986,** *21,* 879.
(20) Helman, M. D.; Carter, D. L.; Gonzalez, C. L. *Soil Sci.* **1965,** *100,* 409.
(21) Bingham, F. T. In *Methods of Soil Analysis, Part 2,* 2nd ed.; Page, A. L., et al., Eds.; American Society of Agronomy: Madison, WI, 1982; pp 431–447.
(22) Cotton, F. A.; Wilkinson, G. *Advanced Inorganic Chemistry,* 5th ed.; Wiley: New York, 1988; Chapter 6, p 169.
(23) Goldberg, S.; Glaubig, R. A. *Soil Sci. Soc. Am. J.* **1985,** *49,* 1374.
(24) Goldberg, S.; Forster, H. S.; Heick, E. L. *Soil Sci.* **1993,** *156,* 316.
(25) Helferrich, F. *Ion Exchange;* McGraw-Hill Book Company: New York, 1962; pp 132 and 139.
(26) Barrow, N. J. *J. Soil Sci.* **1992,** *43,* 37.
(27) Robinson, R. A.; Stokes, R. H. *Electrolyte Solutions,* 2nd ed.; Butterworths: London, 1959; p 518.
(28) Alwitt, R. S. *J. Colloid Interface Sci.* **1972,** *40,* 195.
(29) Beyrouty, C. A.; van Scoyoc, G. E.; Feldkamp, J. R. *Soil Sci. Soc. Am. J.* **1984,** *48,* 284.
(30) Blesa, M. A.; Maroto, A. J. G.; Regazzoni, A. E. *J. Colloid Interface Sci.* **1984,** *99,* 32.
(31) Goldberg, S.; Forster, H. S.; Heick, E. L. *Soil Sci. Soc. Am. J.* **1993,** *57,* 704.
(32) Bloesch, P. M.; Bell, L. C.; Hughes, J. D. *Aust. J. Soil Res.* **1987,** *25,* 377.
(33) Pistorius, C. W. F. T. *J. Chem. Phys.* **1959,** *31,* 1454.
(34) Moenke, H. H. W. In *The Infrared Spectra of Minerals;* Farmer, V. C.; Ed.; Mineralogical Society: London, 1974; pp 365–382.
(35) Kodama, H. *Infrared Spectra of Minerals. Reference Guide to Identification and Characterization of Minerals for the Study of Soils;* Technical Bulletin; Agriculture Canada: Ottawa, 1985; pp 28 and 169.
(36) Tejedor, M. I.; Anderson, M. A. *Langmuir* **1986,** *6,* 602.
(37) Christ, C. L.; Clark, J. R. *Phys. Chem. Miner.* **1977,** *2,* 59.

Received for review February 24, 1994. Revised manuscript received October 6, 1994. Accepted October 14, 1994.[⊗]

ES940113G

[⊗] Abstract published in *Advance ACS Abstracts,* December 1, 1994.